Performance of Closed-Loop Power Control in DS-CDMA Cellular Systems

A. Chockalingam, *Member, IEEE*, Paul Dietrich, Laurence B. Milstein, *Fellow, IEEE*, and Ramesh R. Rao, *Senior Member, IEEE*

***Abstract*—In situations where the round-trip delay between the mobile and the base stations is smaller than the correlation time of the channel, power-control schemes using feedback from the base station can effectively compensate for the fast fading due to multipath. In this paper, we study several closed-loop power-control (CLPC) algorithms by analysis and detailed simulation. We introduce a new loglinear model for analyzing the received power correlation statistics of a CLPC scheme. The model provides analytical expressions for the temporal correlation of the power-controlled channel parameterized by the update rate, loop delay, and vehicle speed. The received power correlation statistics quantify the ability of closed-loop power control to compensate for the time-varying channel. To study more complex update strategies, detailed simulations that estimate the channel bit-error performance are carried out. Simulation results are combined with coding bounds to obtain quasi-analytic estimates of the reverse link capacity in a direct-sequence code-division multiple-access (DS-CDMA) cellular system. The quasi-analytic approach quantifies the performance improvements due to effective power control in both single-cell and multicell DS-CDMA systems operating over both frequency-nonselective and frequency-selective fading channels. The effect of nonstationary base stations on the system performance is also presented.**

***Index Terms*—Cellular systems, closed-loop power control, DS-CDMA.**

I. Introduction

THE USE OF direct-sequence (DS) spread spectrum for code division multiple access (CDMA) cellular communication networks necessitates the use of some form of adaptive power control [1], [2]. Power control provides a means to equalize the received power at the base station of all mobile subscribers within the base station's coverage area. Without such power control, the *near–far effect*—users with large received power at the base station degrading the performance of users with a smaller received power—can drastically limit performance. Closed-loop power-control (CLPC) algorithms use estimates of the received power, measured at the base station, to instruct each mobile to change its transmit power accordingly [3]. CLPC schemes can be effective in compensating for the rapid channel variations due to multipath fading in both terrestrial systems and systems using base stations on-board low-altitude unmanned airborne vehicles (UAV's) in tactical environments, where the propagation and processing delays are small compared to the correlation time of the channel [4].

In traditional voice systems, interleaving and coding are used in conjunction with power control to compensate for the channel burst errors and "mask" the bursty nature of the fading channel at the cost of interleaving and coding delay as well as system complexity [5]. Knowledge of the burst error characteristics of the power-controlled channel can be useful in defining coding and interleaving requirements. Effects of fading and coding on burst errors, packet error rate, and bit-error correlation have been studied recently in [6]–[8], all for nonpower-controlled channels. Similar studies on power-controlled fading channels have not been reported so far. In fact, most reported studies on closed-loop power control for direct-sequence code-division multiple-access (DS-CDMA) systems have, so far, been limited to signal-to-interference ratio (SIR) calculations primarily through simulations, a consequence, apparently, of the intractable nature of the analysis of such systems [3], [9], [10].

In this paper, we study closed-loop power control by both analytical and simulation methods. We introduce a simplified model for analyzing a CLPC system. The model transforms the standard CLPC model into a loglinear model that can be simplified and analyzed as a linear system [11]. From it, we obtain all the first- and second-order received power statistics, i.e., mean, variance, and correlation. Although the received power correlation does not directly specify channel burst error characteristics, it provides insight into the bursty nature of a power-controlled CDMA channel. The received power correlation function quantifies the ability of closed-loop algorithms to dynamically adjust to the time-varying channel. Simplifications are made in forming a tractable analytical model which yields all second moment statistics, and the model accommodates only one type of power-control algorithm. Additionally, several approximations are made in deriving the analytical solution. We therefore construct a simulation of the CLPC system. The simulation validates the accuracy of the analytical model and provides complete performance results for more complex power-control systems and algorithms.

Manuscript received June 3, 1996; revised January 6, 1997. This work was supported in part by the TRW Military Electronics and Avionics Division under Grant NB8541VK2S, Airtouch Communications, Martin Marrieta, the Center for Wireless Communications at the University of California, San Diego, and the MICRO Program of the State of California. This paper was presented in part at the Vehicular Technology Conference, Atlanta, GA, April 1996, and at the 29th Annual Asilomar Conference on Signals, Systems, and Computers, November 1995.

A. Chockalingam is with Qualcomm, Inc., San Diego, CA 92121 USA.

P. Dietrich is with Metricom, Los Gatos, CA 95030 USA.

L. B. Milstein and R. R. Rao are with the Department of Electrical and Computer Engineering, University of California, San Diego, La Jolla, CA 92093 USA.

Publisher Item Identifier S 0018-9545(98)02479-7.

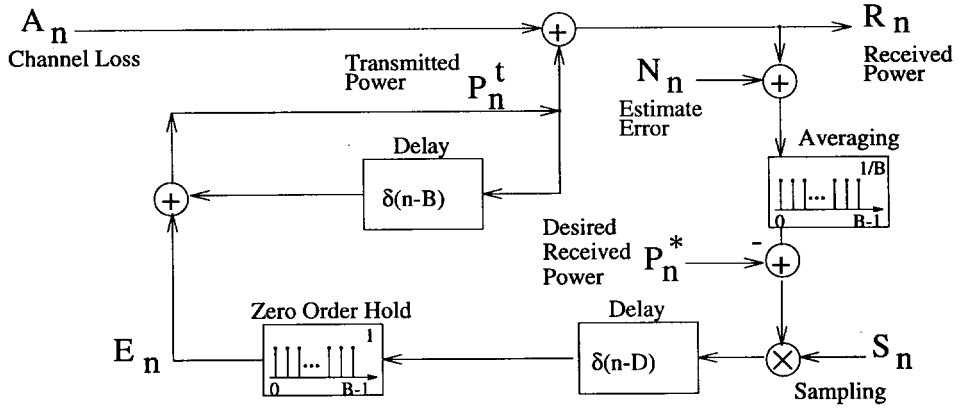

Fig. 1. Loglinear power-control model.

Combining the simulation results with coding bounds to form a quasi-analytic approach, we estimate the reverse link (mobile-to-base-station link) capacity of a DS-CDMA system that employs closed-loop power control. Unlike the previous studies on closed-loop power control which estimated mainly the SIR statistics [3], [9], our present study estimates the capacity based on the channel bit-error rate (BER) (uncoded), which is obtained through large-scale simulations, and analytical bounds on the coded BER performance. For this study, we consider a voice system whose link quality requirement in terms of coded BER is typically of the order of 10^{-3}, and our capacity estimates are subject to meeting this requirement. We consider both a single- as well as a multicell system (25 cells in a square grid layout) operating over both frequency-nonselective (flat) and frequency-selective Rayleigh fading channels. The reverse link capacity in a multicell environment has been investigated by many authors [1], [12], [13]. Most of these studies, for analytical simplicity, assume that a mobile talks to a base station which is nearest to it, and further, that the base stations do not move. In fact, the nearest base station need not always be the best choice because of the losses due to fading and shadowing. It is more appropriate to consider the average received signal power (which is a function of both distance and shadow losses) as the criterion for the base-station assignment. In [14], we showed that a base-station assignment strategy, based on a maximum received power criterion, performed significantly better than the one using a minimum distance criterion, both under stationary and nonstationary base-station scenarios. Note that mobile base stations may be necessary for providing an effective communications infrastructure in tactical and emergency communications environments. Base stations, under such situations, could be mounted on moving platforms like jeeps, tanks, UAV's, etc. In this paper, we estimate the performance of closed-loop power control in a mobile base-station scenario. We allow the cell-of-interest to move with respect to two tiers of interfering cells and estimate the reverse link capacity at the moving cell as a function of fractional cell overlap.

The rest of the paper is organized as follows. In Section II, we describe the loglinear power-control model and present the analysis to derive the received power autocovariance function. Numerical results from both analysis and simulation are presented and compared. Section III presents the average BER performance of the CLPC system as a function of various loop parameters, including power-control update rate, loop delay (due to propagation and processing), and vehicle speed. In Section IV, the reverse link capacity of a closed-loop power-controlled DS-CDMA system in a multicell environment is estimated for both stationary and nonstationary base-station scenarios. Section V provides the conclusions.

II. Loglinear Power-Control Model

Consider the loglinear power-control model shown in Fig. 1. All sequences marked represent power in decibels at a particular point. The subscript n in all the expressions indexes bits. The boxes represent linear filters, marked by either a fixed delay or filter impulse response. This figure represents a linear system model for a single mobile-to-base-station link. The model captures only the instantaneous powers at various points in the system and not the actual signals. The nth bit is transmitted with power P_n^t, but not all energy transmitted in bit n is received. Power is lost due to fading represented by adding a channel loss A_n, which is constant over the bit. A_n has a value equal to $10\log_{10}(a_n^2)$, where a_n has a Rayleigh distribution. The logarithm transforms fades ($a_n < 1$) into negative values of A_n. The statistics of the sequence A_n are given in Appendix A. Implicit in this description is the assumption that the underlying fading process $a(t)$ is frequency nonselective and does not vary rapidly with respect to a single bit time. Additional loss is due to propagation distance and shadowing. These phenomena are relatively slow as compared to the fading process, so it is assumed that they are "tracked out" perfectly by the power-control algorithm. If more complex models including shadowing, fading, and mobility are desired, additional channel loss processes could be added.

The nth bit is received at the base station with power R_n, where R_n represents the actual power in the received signal of interest. This is not typically a measurable quantity, as it does not include the error involved in estimating this power. Analytically, however, the quantity R_n is of primary interest, since it represents the true power of the desired signal. The base station is assumed to measure power by examining the

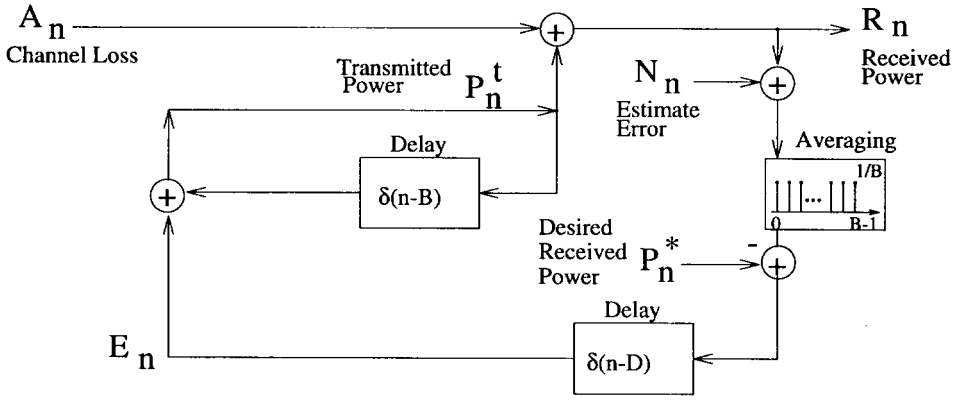

Fig. 2. Simplified loglinear power-control model.

square of the test statistic for each bit. Because thermal noise in the receiver and power from other mobiles is also received, the estimate for received power contains some error. This error (in decibels) is modeled by the process N_n. Because the square of the test statistic is used as an estimate for power, the estimate is biased and, thus, the process N_n has a nonzero mean. The sequence N_n must not be confused with the thermal noise process at the receiver: N_n is strictly a power estimate error. It is not immediately evident what the characteristics of such a process are. The modeling of the process N_n is given in Appendix B.

The base station averages the samples $R_n + N_n$ over B bits, as shown by the averaging filter, and uses this estimate of the power to enforce power level changes at the mobile. The correction applied to the mobile's power is obtained by subtracting this estimate from the desired received power P_n^* (e.g., if the received power is too large, the correction is negative). The sampling waveform

$$S_n = \sum_{i=0}^{\infty} \delta_{n-iB} \tag{1}$$

where

$$\delta_x = \begin{cases} 1, & x = 0 \\ 0, & \text{otherwise} \end{cases} \tag{2}$$

samples this average power correction once every B bits. This is the value that is used by the mobile for updating its transmit power. Due to round-trip propagation, processing, and frame delay, it is assumed that this correction can be used by the mobile D bits after it is computed. The mobile, using a zero-order hold, reconstructs the desired change in power suggested by the base station and adds it to its transmitted power from B bits previous (i.e., adding the correction to the old transmit power yields a new transmit power P_n^t that, one hopes, is more accurate).

This model captures the time evolution of the power-control update process. By constructing suitable input processes (i.e., A_n, N_n, and P_n^*), one can determine the statistics of the received power level R_n. Also, the model can be modified to consider other update algorithms. For example, to construct an update algorithm where the transmit power is raised or lowered by some fixed amount, regardless of the magnitude of the power-control error, one could add a suitable *nonlinearity* after the sampling signal. However, the consideration of other update strategies leads to significantly more complicated analysis, and therefore these latter update strategies are examined by simulation in Section III. For simplicity of analysis, we model and analyze an *inverse update algorithm* which increases or decreases the mobile user's transmit power by the actual difference between the received signal power and the desired received signal power. The channel is assumed to undergo flat Rayleigh fading, with a Doppler spectrum of the form [15]

$$a(f) = \begin{cases} \dfrac{1}{2\pi f_d \sqrt{1-\left(\dfrac{f}{f_d}\right)^2}}, & |f| < f_d \\ 0, & \text{elsewhere} \end{cases} \tag{3}$$

so that the underlying Gaussian processes have normalized correlation functions given by $J_0(2\pi f_d \tau)$, where $J_0(.)$ is the Bessel function of the first kind of order zero, $f_d = v/\lambda$ is the Doppler bandwidth, v is the vehicle speed, λ is the wavelength, and τ is the time delay between the specified correlated samples. The interfering users are assumed to be seen at the receiver with perfect power control, i.e., their received power is fixed at P^*. These interfering users' signals contribute to the received power estimation error of the user-of-interest.

A. Analysis

The linear system model shown in Fig. 1 contains a sampling waveform. Here, for simplicity of results, we consider a modified linear system model, shown in Fig. 2, that captures the essence of this sampled system. Because the sampling and zero-order hold reconstruction have been removed, the mobile has better knowledge of its received power. Thus, this approximation is likely to yield a system that performs better than the actual sampled system.

In this simple linear model, we can use superposition. Hence, we find the transfer function for each of the inputs A_n, P_n^*, and N_n. For example, setting P_n^* and N_n to zero, we can solve for the transfer function $H_{RA}(\Omega) = R(\Omega)/A(\Omega)$. $A(\Omega)$ and $R(\Omega)$ are the discrete Fourier transforms of A_n and R_n, respectively. Assuming a deterministic signal for A_n, we can write

$$R(\Omega) = P^t(\Omega) + A(\Omega) \tag{4}$$

$$P^t(\Omega) = P^t(\Omega)e^{-j\Omega B} + E(\Omega) \tag{5}$$

and

$$E(\Omega) = -H_f(\Omega)R(\Omega)e^{-j\Omega D} \tag{6}$$

where $H_f(\Omega)$ is the Fourier transform of the B bit averaging filter. Solving for $R(\Omega)$ in terms of $A(\Omega)$ yields

$$H_{RA}(\Omega) = \frac{(1 - e^{-j\Omega B})}{1 - e^{-j\Omega B} + H_f(\Omega)e^{-j\Omega D}} \tag{7}$$

where [16]

$$H_f(\Omega) = \frac{1}{B}\frac{\sin(\Omega B/2)}{\sin(\Omega/2)}e^{-j\Omega[(B-1)/2]}. \tag{8}$$

Similarly, we can find $H_{RN}(\Omega)$ and $H_{RP^*}(\Omega)$. They can be expressed as

$$H_{RN}(\Omega) = \frac{-H_f(\Omega)e^{-j\Omega D}}{1 - e^{-j\Omega B} + H_f(\Omega)e^{-j\Omega D}} \tag{9}$$

and

$$H_{RP^*}(\Omega) = \frac{1}{1 - e^{-j\Omega B} + H_f(\Omega)e^{-j\Omega D}} \tag{10}$$

respectively.

We are interested in the correlation of R_n, the received power at the base station. As a measure of received power correlation, we consider the autocovariance function of the sequence R_n

$$\mathrm{Cov}[R_j, R_{j-i}] = E[R_jR_{j-i}] - E[R_j]E[R_{j-i}]. \tag{11}$$

Since this system has been modeled as linear, we can use superposition and represent the sequence R_n as a sum of three sequences due to the three inputs P_n^*, A_n, and N_n, which we shall denote as R_n^P, R_n^A, and R_n^N, respectively. In other words, $R_n = R_n^P + R_n^A + R_n^N$.

The sequence P_n^* is a constant, and thus the sequence R_n^P is deterministic and independent of R_n^A and R_n^N (if P_n^* varies, possibly to control the intercell interference, the correlation of P_n^* must be appropriately modeled). The sequences R_n^A and R_n^N are not independent. The power of the noise interference term to be given in Appendix B has been shown to depend on the received power of the user-of-interest. This is clearly a function of A_n and also, indirectly, a function of N_i, $i \leq n$. A simple approximation that removes this correlation is given in Appendix B. Based on the assumed independence of R_n^A, R_n^N, and R_n^P, the autocovariance of R_n is the sum of the autocovariances of R_n^A, R_n^N, and R_n^P, i.e.,

$$\begin{aligned}\mathrm{Cov}[R_j, R_{j-i}] = {} & \mathrm{Cov}[R_j^P, R_{j-i}^P] + \mathrm{Cov}[R_j^A, R_{j-i}^A] \\ & + \mathrm{Cov}[R_j^N, R_{j-i}^N].\end{aligned} \tag{12}$$

From this, it follows that

$$\begin{aligned}S_R(\Omega) \triangleq {} & \mathcal{F}(\mathrm{Cov}[R_j, R_{j-i}]) \\ = {} & |H_{RA}(\Omega)|^2 S_A(\Omega) + |H_{RN}(\Omega)|^2 S_N(\Omega) \\ & + |H_{RP^*}(\Omega)|^2 S_P(\Omega)\end{aligned} \tag{13}$$

where $S_A(\Omega)$, $S_N(\Omega)$, and $S_P(\Omega)$ are the power spectra of the sequences A_n, N_n, and P_n^*, respectively. If we can find the correlation functions, and, consequently, the power spectra, of the "inputs" to the linear system, we can find an expression for the received power correlation at the base station. Since the autocovariance function of P_n^* is equal to zero, the above expression reduces to

$$S_R(\Omega) = |H_{RA}(\Omega)|^2 S_A(\Omega) + |H_{RN}(\Omega)|^2 S_N(\Omega). \tag{14}$$

The derivation of the autocovariance function of A_n is given in Appendix A. In Appendix B, we construct the loglinear noise model N_n and derive the mean and variance of the process N_n subject to two major approximations. The validity of those approximations is also examined in Appendix B.

B. Results

Interleaving and coding are typically used to combat the effect of burstiness in a mobile radio channel. The effect of interleaving is to scramble the bits so as to disperse bursts of errors over a large number of bits. Since the most powerful codes, typically, work best on independent identically distributed (i.i.d) channels, a code is applied before interleaving so that the deinterleaved bits that enter the decoder have errors that appear to be i.i.d. It is important that the depth of the interleaver be such that bursts of errors are spread sufficiently so that a single burst cannot overwhelm the decoder. To determine the interleaving depth, a designer requires knowledge of the burst error statistics of the channel. Burst errors occur when the received power falls below an acceptable level for a period that spans many bits. The received power autocovariance can be used to find approximations for these statistics, as the degree of correlation is related to the burst length statistics.

The received power correlation is computed for various values of the parameters B, f_d, and D. The input correlation and the transfer function of the linear system are known in closed form only in the time domain. Numerical computation is required to perform the time domain convolution. In generating the following results, 2^{14} point fast Fourier transforms (FFT's) were used to compute the linear system output. The effect of the averaging interval B on the received power correlation, as predicted by the above analysis, is shown in Fig. 3 for $f_d = 25$ Hz (corresponding to 30-km/h vehicle speed at 900-MHz carrier frequency) and $D = 5$. The received power autocovariance is also shown for the flat Rayleigh fading channel without power control. As the power is updated less frequently, the correlation in received power increases in magnitude and duration. In the limit as B grows large, the received signal power approaches that of the flat Rayleigh fading channel without power control. As the power-control update can require significant bandwidth, it is desirable to keep B as large as possible without sacrificing performance. Even in this ideal power-control model, for reasonable B, the closed-loop power control does not remove all of the "burstiness" or received power correlation present in the channel. These curves quantify the increase in correlation time as well as the increase in variance due to lengthening the update interval. The curves further imply that smaller depth interleavers could be used in a power-controlled channel, since the autocovariance with power control spans shorter time intervals (e.g., over 50-b

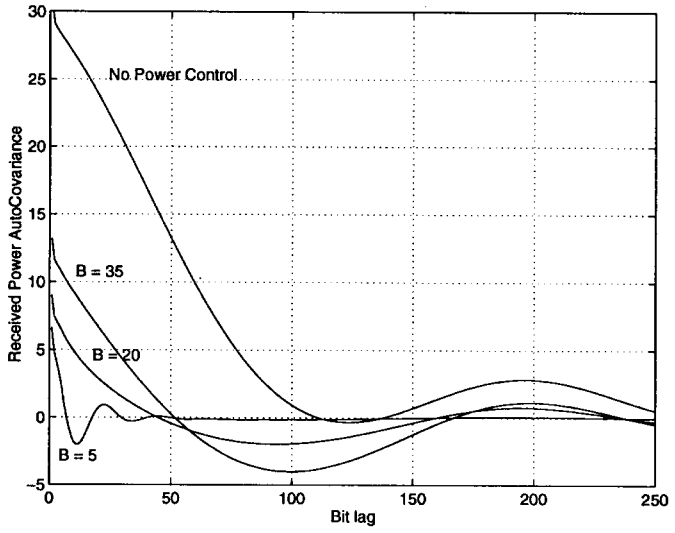

Fig. 3. Effect of averaging interval B on the received power autocovariance for $f_d = 25$ Hz and $D = 5$.

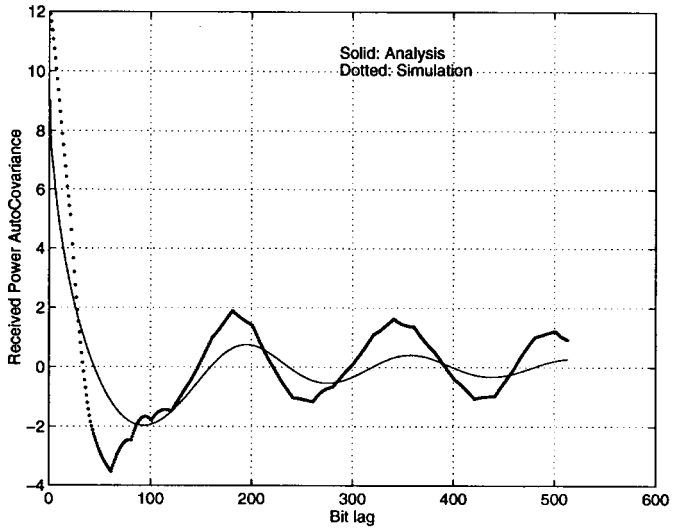

Fig. 4. Comparison of received power autocovariance function as predicted by analysis and simulation for $f_d = 25$ Hz, $B = 20$, $E_b/N_o = 10$ dB, $D = 5$, and $T_b = 1/8000$ s.

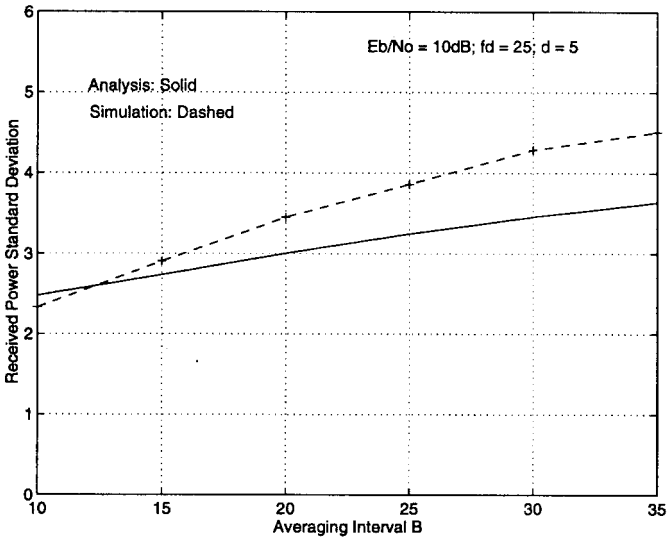

Fig. 5. Comparison of received power standard deviation as predicted by analysis and simulation for $f_d = 25$ Hz, $E_b/N_o = 10$ dB, $D = 5$, and $T_b = 1/8000$ s.

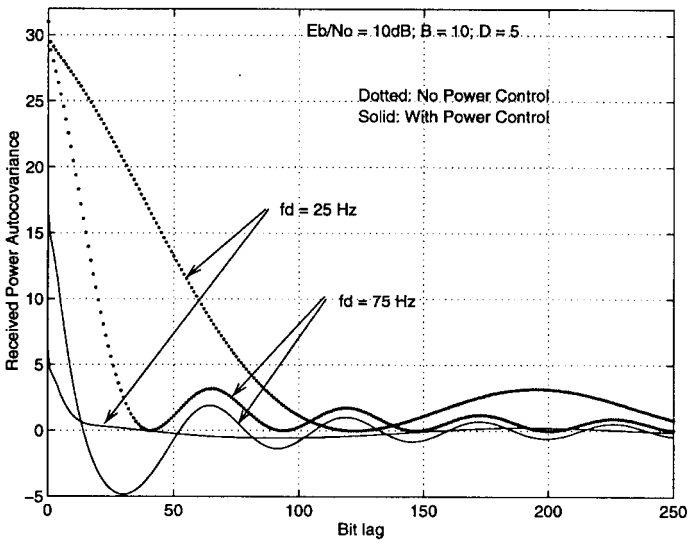

Fig. 6. The effect on the received power autocovariance function as a result of increasing Doppler frequency, f_d (Hz). $B = 10$, $D = 5$, $E_b/N_o = 10$ dB, and $T_b = 1/8000$ s.

lag for $B = 35$) than it does without power control (over 100-b lag).

The approximations made in forming the loglinear model are found to have an impact on the performance results. Fig. 4 shows the autocovariance as predicted both by the analysis and by simulation. The curves, although similar in shape, differ in the magnitudes of their correlations. The simulated correlation function shows the effect of sending the average received power only once every B bits. The resulting correlation function is composed of B-bit segments connected to form a jagged curve (Fig. 4 at around 100 b of lag). Because the linear model presented here removes the sample-and-hold (Fig. 2), the analysis curves fail to reflect this phenomenon. It is presumed that this modeling assumption not only effects the shape, but also has an impact on the magnitude of the correlation function. The standard deviation of the received power is shown in Fig. 5. For averaging intervals B less than 20 (i.e., fast power-control updates), the analysis predicts a standard deviation with better than 0.5-dB accuracy compared to the simulation results. In fact, for most practical update rates (e.g., $B = 10$, corresponding to an update rate of 800 Hz, as in IS-95), the prediction accuracy is less than 0.25 dB. For $B > 30$, the prediction accuracy is around 1 dB. Also, over this entire range, the shape of the correlation function, and thus, the duration of the time correlation, is predicted well by the analysis (Fig. 4), which is useful in understanding the burst error statistics.

Fig. 6 shows the effect of increasing the Doppler frequency f_d (equivalently, increasing vehicle speed) on the received power covariance when $B = 10$ and $D = 5$. In a Rayleigh fading environment with no power control, increasing vehicle speed results in a decrease in the "length" of the channel

autocovariance while the received power variance at 0-b lag remains constant (Fig. 6, dotted lines). When the vehicle speed is sufficiently fast, the channel autocovariance tends toward a delta function—received signal power is approximately independent from bit to bit. When the vehicle speed slows to zero, the channel autocovariance is a constant $100\pi^2/6 \ln^2 10$. This constant comes directly from the computation of the Rayleigh fading power autocovariance function. The zero lag of this function equals the variance of the fading power at any given time. At zero vehicle speed, the fading loss remains constant for each realization of the random process—the fading loss is a single random variable with variance $100\pi^2/6 \ln^2 10$.

In the power-controlled Rayleigh fading environment with fixed B and D, increasing the vehicle speed results in an *increase* in the magnitude of the highest peak in the autocovariance (Fig. 6, solid lines). Note that for slow vehicle speed the channel autocovariance function is almost zero. In a slowly varying environment, the fading is tracked perfectly, with only small variations due to the noise in the received power estimate (Fig. 6, $f_d = 25$ Hz). Power control removes almost all random variations in the received signal power. As the vehicle speed increases, the combined effect of the interval B and delay D causes the power-control updates to become increasingly stale. That is, the channel has already changed significantly by the time an update is applied at the mobile. This, in turn, causes an increase in the received power variance, and an increase in the duration of the received power autocovariance (Fig. 6, $f_d = 75$ Hz).

III. CLPC BER Performance

The method presented in Section II provides analytical results that are easy to compute and interpret. Moderate computing resources can generate results for a single parameter set in less than a minute, making it more attractive than statistical simulation. However, the model is not easily extended to directly provide bit-error characteristics. To complement the analytic results, we use simulations to investigate bit-error performance of the power-control algorithms.

We initially examine the average bit-error performance of just a single user CLPC system operating over a flat Rayleigh fading channel. Although the primary idea behind power control is obviously to equalize the powers from multiple users, estimating the performance of a single power-controlled user is useful to quantitatively predict the effectiveness of the loop in tracking the fast fading, and the contribution of each element in the loop to the overall system performance. Bit-error measurements through simulations are carried out to establish the effect of parameters such as power update step size (adaptive versus fixed), power-control update rate, propagation and processing delay in the loop, and vehicle speed on the average BER performance. The simulated system considers an information rate of 8 Kbps, such that a B value of 20 corresponds to a 400-Hz update rate, 10 corresponds to 800 Hz, 5 corresponds to 1.6 kHz, and so on. Similarly, a D value of 20 corresponds to a loop delay of 2.5 ms, 10 corresponds to 1.25 ms, and so on. The P^* value is set to be the desired E_b/N_o.

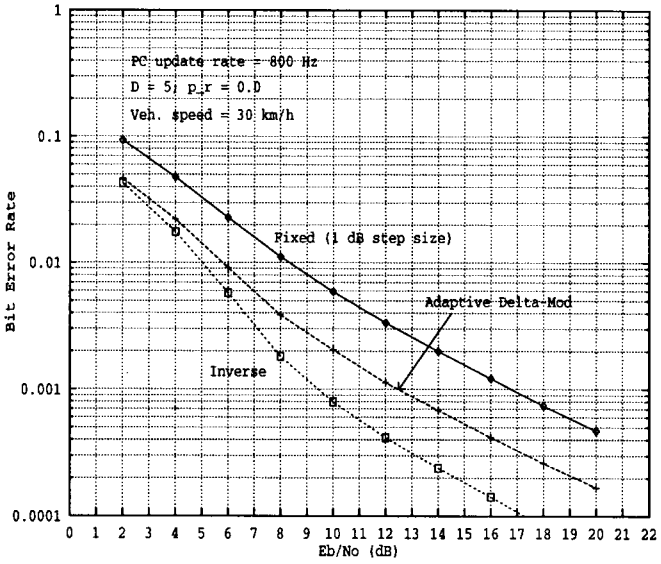

Fig. 7. Comparison of the BER performance of fixed step size, adaptive delta modulation, and inverse algorithms. Flat Rayleigh fading. $P^* = E_b/N_o$. Update rate $= 800$ Hz.

As noted earlier, the transmit power update step size can be either fixed (*fixed step size algorithm*) or made adaptive to the channel variations. A specific example of the adaptive step size approach is the *inverse algorithm* as defined in Section II. Fixed step size algorithms are easy to implement, and need much less bandwidth on the forward link (base-to-mobile link). This is because only the sense of power change (i.e., up or down) needs to be conveyed to the mobile, which can be achieved by sending a simple 1-b command, which we assume can be in error with probability p_r. Fig. 7 shows a performance comparison between the fixed step size algorithm, an adaptive delta-modulation algorithm, and the inverse algorithm. A step size Δ of 1 dB is used in the fixed step size algorithm. An update rate of 800 Hz, a vehicle speed of 30 km/h (corresponding to a Doppler frequency of 25 Hz, considering a carrier frequency of 900 MHz), and a return channel error rate p_r of 0.0 are used. As expected, the performance of the inverse algorithm is found to be superior to that of the fixed step size algorithm. For example, for the above set of parameters, the inverse algorithm needs 3.5 dB less E_b/N_o than the fixed step size algorithm to achieve 10^{-2} BER. Inverse algorithm implementations, however, would need additional bandwidth on the return channel to carry the power-control step size, in addition to the power up/down command. In practice, because of the increased complexity and bandwidth requirements, inverse algorithms are rarely used. A compromise would be to use an adaptive delta-modulation algorithm. In all our following simulations, we will focus on the fixed step size algorithm.

The effect of power-control update rate on the BER performance is illustrated in Fig. 8, when the vehicle speed is 30 km/h, $\Delta = 1$ dB, $D = 0$, and $p_r = 0.0$. The results are plotted for different update rates, 200, 400, and 800 Hz, and 1.6 kHz, corresponding to $B = 40$, 20, 10, and 5 b, respectively. The performance plots corresponding to both an additive white Gaussian noise (AWGN) channel and a flat fading channel

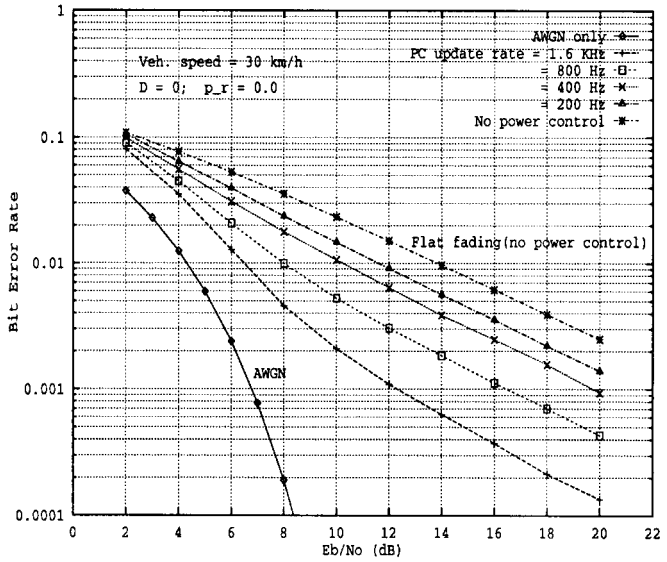

Fig. 8. Bit-error rate versus E_b/N_o as a function of power-control update rate. Flat Rayleigh fading. $P^* = E_b/N_o$. $\Delta = 1$ dB.

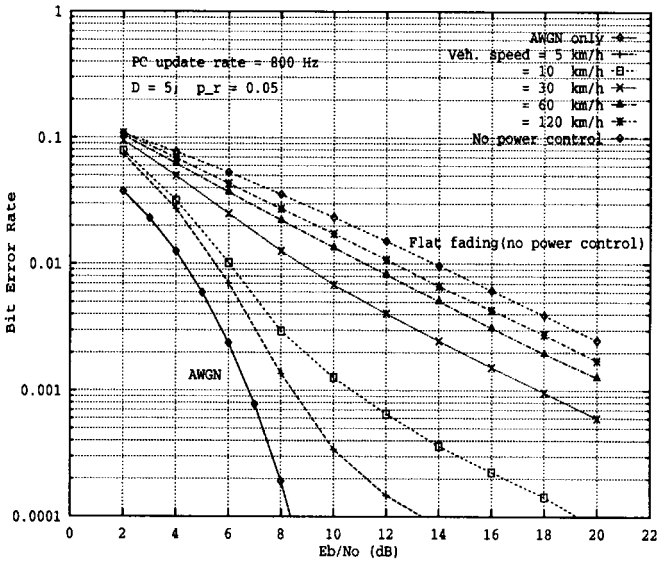

Fig. 9. Bit-error rate versus E_b/N_o as a function of vehicle speed. Flat Rayleigh fading. $P^* = E_b/N_o$. $\Delta = 1$ dB. Update rate $= 800$ Hz.

without power control are also shown for comparison. As can be seen, the performance curves shift closer to the AWGN-only performance as the update rate is increased. On the other hand, slower updates tend to result in performance which is increasingly closer to fading performance with no power control. For example, when the channel fading is flat, and no power control is employed, a BER performance of 10^{-2} is achieved at an E_b/N_o of 14 dB—the same performance is achieved with E_b/N_o of 11.6 and 6.5 dB for update rates of 200 Hz and 1.6 kHz, respectively. The tradeoff here is that power control is more effective at faster update rates, but at the expense of a proportionately larger bandwidth that is needed on the return channel to carry the command bit more frequently. Again, an effective update rate is, in a sense, relative to the rate at which the channel fades, which is a function of the Doppler bandwidth (hence, the vehicle velocity). The effect of different vehicle speeds on the BER performance at a constant update rate of 800 Hz is shown in Fig. 9. The range of vehicle speeds considered spans from typical pedestrian speeds (5 km/h) to freeway speeds (120 km/h). At pedestrian speeds, the power control is seen to be very effective such that at 10^{-2} BER, the power-control performance is just about 1.5 dB poorer than the AWGN-only performance. This is due to the high correlation time of the channel at low vehicle speeds. The channel correlation time decreases as the vehicle speed increases, thus degrading the performance. It is to be noted that what is illustrated in Fig. 9 is the effect of power control alone as a function of speed, and what is not brought out is the effect of interleaving which, in practice, is incorporated in the system design to randomize the burstiness of the channel errors in a fading environment. At low speeds, although power control is very effective, interleaving is ineffective—the reverse is true at high vehicle speeds, i.e., power control does not track fades effectively, whereas interleaving becomes efficient. The net effect is that the performance degrades up to a certain speed, and beyond that speed the performance improves. This is a classical power-control/interleaving performance tradeoff [5].

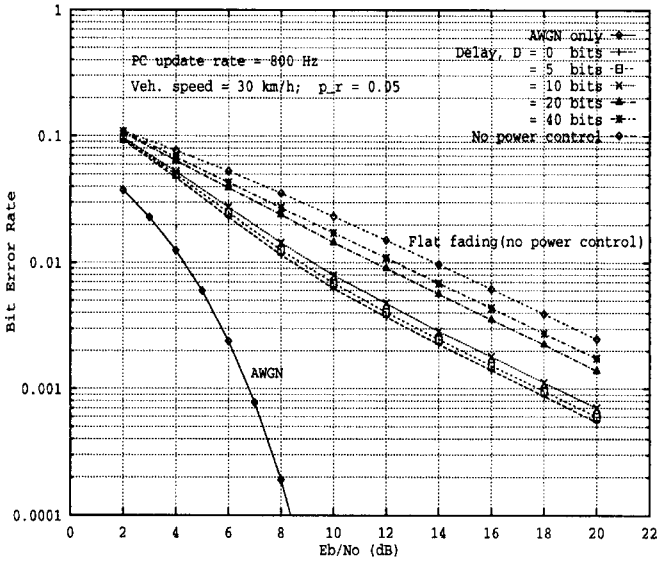

Fig. 10. Bit-error rate versus E_b/N_o as a function of return channel delay. Flat Rayleigh fading. $P^* = E_b/N_o$. $\Delta = 1$ dB. Update rate $= 800$ Hz.

In [20], for a power-controlled DS-CDMA system with rate-1/3 convolutional coding, 32×18 block interleaving, and two-ray antenna diversity at the base station, the worst case performance is shown to occur at 60-km/h vehicle speed.

Another critical parameter in the power-control loop is the delay due to propagation and processing. Fig. 10 shows the effect of the propagation and processing delays (D) on the BER performance for an update rate of 800 Hz, vehicle speed of 30 km/h, $\Delta = 1$ dB, and $p_r = 5\%$. The range of values considered for the parameter D is 0–40 b, which corresponds to loop delays in the range of 0–5 ms. The curve corresponding to $D = 0$ represents the performance when the power-control command is available at the mobile almost instantaneously, in other words, when the loop delay is very small compared to the bit duration. For loop delays

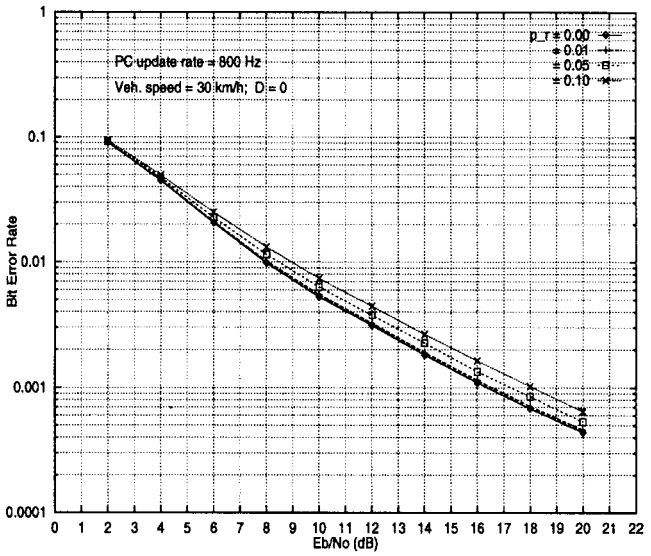

Fig. 11. Bit-error rate versus E_b/N_o as a function of return channel error rate (p_r). Flat Rayleigh fading. $P^* = E_b/N_o$. $\Delta = 1$ dB. Update rate $= 800$ Hz.

up to $D = 10$ (i.e., 1.25 ms), the performance degradation is not very significant. In fact, at 10^{-2} BER, the performance difference between $D = 0$ and 10 is just 0.5 dB. The above results and other simulation results at different speeds and update rates lead to the observation that while closed-loop power control will be effective in terrestrial cellular systems, it will not be effective on satellite links. However, it can be useful for systems employing base-stations on-board UAV's, since UAV's are typically placed at altitudes in the range 20–30 km (with corresponding round-trip propagation delays of about 0.2 ms). Fig. 10 also shows a sharp performance degradation for $D > 10$. For example, when $D = 20$, the performance worsens by around 4 dB compared to $D = 0$ at 10^{-2} BER. This is due to the fact that when the loop delay becomes greater than the channel correlation time, the power-control updates become less meaningful. While there is nothing that can be done about the delay due to propagation, the delay due to processing, in a practical system, can be minimized by making the received power measurements before the deinterleaver [3].

To reduce the processing delay and to save bandwidth on the forward link, the command bit from the base station is not always error protected. Thus, it becomes necessary to understand the effect of the channel error rate of these unprotected bits on the performance. Simulations were run at different return channel error probabilities, namely $p_r = 0.0\%$, 1%, 5%, and 10%, and Fig. 11 shows the BER versus E_b/N_o plot parameterized by the p_r values. It is seen that the error rate on the return channel has little effect on the performance. In fact, at an update rate of 800 Hz and a vehicle speed of 30 km/h, the performance degradation is just 0.5 and 1 dB for p_r of 5% and 10%, respectively, compared to an error-free return channel (i.e., $p_r = 0.0$).

IV. Single-Cell/Multicell Reverse Link Capacity

In this section, we consider the estimation of reverse link capacity in a DS-CDMA cellular system employing closed-loop power control. We estimate capacity both for a single-cell system as well as a multicell system, considering both flat and frequency-selective channel models. The effect of different power-control update rates and vehicle speeds on the reverse link capacity is evaluated, as well as the effect of nonstationary base stations. The approach we adopt to estimate capacity is *quasi-analytic* in nature, as outlined below.

A. Quasi-Analytic Approach to Capacity Estimation

Practical DS-CDMA systems rely heavily on coding to improve the bit-error performance on the reverse link (e.g., a rate-1/3 convolutional code is used link in IS-95 [1]). Hence, we need to estimate the coded bit-error performance in order to obtain the reverse link capacity estimates. Deriving the coded BER performance through analytical means alone is complex, particularly when moving base stations are considered in the system. Simulation techniques using Monte Carlo and importance sampling approaches are common [21]. Monte Carlo simulation of coded systems take prohibitively long run times. However, from the basic properties of the code, it is possible to calculate an approximation to, or a bound on, the coded BER performance based on the BER at the decoder input,[1] which, in turn, is obtained through simulations. We adopt such a quasi-analytic approach to estimate the reverse link capacity.

We first estimate the channel BER of the DS-CDMA system at different system parameter settings through large-scale simulations. The occurrence of bit errors in such simulation experiments would be *bursty* due to sudden and deep fades appearing on the channel. In practice, the bursty nature of the errors due to the memory on the channel can be manipulated to appear as independent *random errors* by interleaving the coded data over sufficient depth before transmission, and deinterleaving the data before decoding at the receiver. Here, we assume *perfect interleaving* and evaluate an upper bound on the coded bit-error performance of the system using convolutional codes with hard decision Viterbi decoding. This yields the well known transfer function bound

$$p_o < \sum_{i=x_f}^{\infty} \beta_i P(i) \tag{15}$$

where x_f is the free distance of the code and $\{\beta_i\}$ are the coefficients in the expansion of the derivative of $T(D, N)$, the transfer function (or generating function) of the code evaluated at $N = 1$ [22]. $P(i)$ is the probability of selecting the incorrect path, and can be bounded by the expression

$$P(i) < [4p_c(1 - p_c)]^{i/2} \tag{16}$$

where p_c is the channel BER. The tightness of the bounds in (15) and (16) is discussed in [22]. From the coded bit-error performance, we then estimate the *system capacity*, which is defined as the number of simultaneous users that can be supported while maintaining an acceptable coded BER performance needed by the specific application (e.g., 10^{-3} for voice). A similar approach could be taken to estimate

[1] We refer to the BER at the Viterbi decoder input as the *channel BER*, p_c.

performance with soft decision decoding (which is expected to perform better than hard decision decoding), provided that the simulation is used to generate the probabilities of the channel transition probability matrix instead of the channel BER [21]. Since our simulations primarily generate the channel BER, we restrict our results to hard decision decoding. It can be realized that there is some element of both optimism and pessimism built in to this approach: optimism due to the perfect interleaving assumption and pessimism because of hard decision decoding instead of soft decision.

B. Channel Model

We model the time-variant channel as a tapped delay line with tap spacing T_c (the chip duration) and tap coefficients $\{z_l(t)\}$ which are zero-mean complex-valued stationary mutually independent Gaussian random processes [22]. Thus, the complex low-pass equivalent channel impulse response is given by

$$h(\tau; t) = \sum_{l=0}^{L_p-1} z_l(t)\delta(\tau - lT_c) \tag{17}$$

where L_p is the number of resolvable paths, each spaced T_c apart. If the multipath spread is T_m, then the number of resolvable paths is $L_p = \lfloor T_m/T_c \rfloor + 1$, and T_m is assumed to be less than T, where T is the bit interval. We can also write $z_l(t) = \alpha_l(t)e^{j\phi_l(t)}$, where the $\{\alpha_l(t)\}$ are Rayleigh distributed and the phases $\{\phi_l(t)\}$ are uniformly distributed in $[0, 2\pi]$. The average path strength Ω_l is the second moment of α_l (i.e., $\Omega_l = E[(\alpha_l)^2]$) and is assumed to be related to the second moment of the initial path strength by

$$\Omega_l = \Omega_0 e^{-\mu l}, \qquad \mu \geq 0. \tag{18}$$

Equation (18) describes the decay of the average path strength as a function of path delay—the parameter μ reflects the rate at which this decay occurs. The shape of the decay function is referred to as the multipath intensity profile, which is assumed to be exponential in our study [23]. Note that the channel model described above corresponds to a flat (frequency nonselective) fading model when $L_p = 1$. The total received powers in both flat fading ($L_p = 1$) and frequency-selective fading ($L_p > 1$) are taken to be the same. We assume that all the resolvable paths are combined coherently with a RAKE receiver [22].

C. System Model

A 25-cell square grid DS-CDMA cellular system, with base stations $\{B_1, B_2, \cdots, B_{25}\}$ and cell boundaries as shown in Fig. 12, is considered. The cell-of-interest B_{13} is surrounded by two tiers of interfering cells. Each cell has J mobile asynchronous users which are uniformly distributed over the cell area. Each user communicates with its assigned base station, on the reverse link, using coherent binary phase-shift keying (BPSK) modulation, rate-1/3 convolutional coding, and direct sequence spreading. Each user is assigned a unique spreading sequence, and the spreading sequences have a common chip rate of $1/T_c$, where $T_c = T/N_c$. T and T_c are the

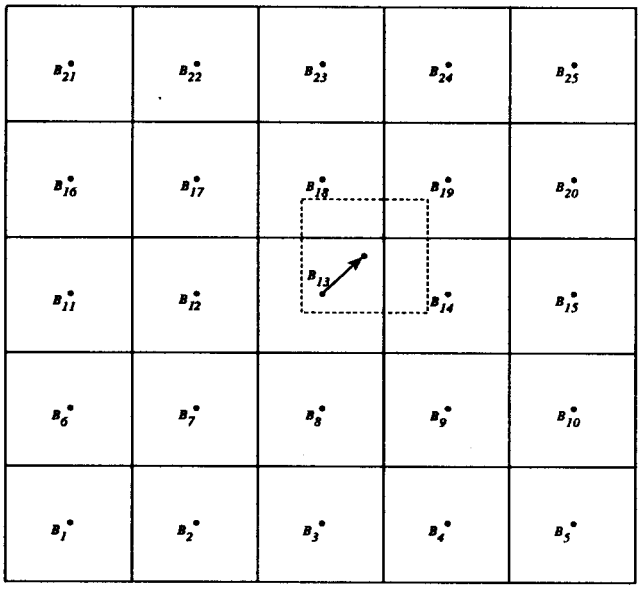

Fig. 12. Twenty-five-cell square grid layout.

coded symbol and chip durations, respectively, and N_c is the number of chips/coded symbol. In the simulations, random binary sequences of length 127 are used as the spreading sequences for different mobiles. All the mobile users are power controlled by their assigned base stations. The assignment of base stations to mobiles is based on a maximum received power criterion; that is, a mobile is assigned to that base station from which it receives maximum signal strength. This strength can be measured on pilot signals which are generally broadcast by the base stations at a constant power to enable the mobiles to achieve synchronization. Distance and shadow losses affect the received signal strength in such a way that is proportional to $10^{\zeta/10}d^{-\nu}$, where d is the distance between the mobile and the base station, and ζ represents the shadow parameter, which is a Gaussian random variable with zero mean and standard deviation σ_s dB. Typically, ν is in the range 2–5.5, and σ_s is in the range 4–12 dB, depending on the environment [15]. In line with [1], a propagation exponent value (ν) of four and a standard deviation of the lognormal shadowing (σ_s) of 8 dB are used in all the simulations. All the mobiles are assumed to be moving at the same speed over a small geographical area, to use the same update rate, and to experience the same delay and error rate on the return channel from their respective base stations. A fixed step size power-control algorithm with $\Delta = 1$ dB is used throughout. In the simulations, the power-control commands for all the mobiles are generated by their assigned base stations based on perfect estimates of the received signal power. Furthermore, coherent demodulation and perfect synchronization are assumed at the receiver.

D. Simulation

A set of CDMA simulation tools developed in C language has been used to synthesize the simulation programs and estimate the channel BER performance p_c under different system conditions. A waveform sampling frequency corresponding

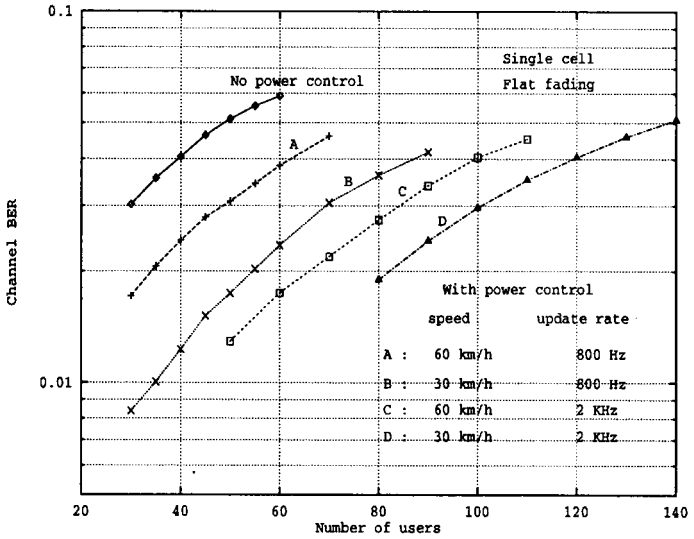

Fig. 13. Channel BER performance of the CLPC scheme in a single-cell DS-CDMA system over a flat Rayleigh fading channel.

to four samples per chip is used. The following strategy is adopted to simulate the slow lognormal shadowing and the fast Rayleigh fading. Over each simulation iteration, a new lognormal shadow variable is generated and held constant over that iteration. However, within each iteration interval, a time-varying Rayleigh fading component is generated following the Doppler spectrum in (3). Power control is implemented to track out this Rayleigh component. The iteration interval is taken long enough to cover several deep fades. A number of such iterations are run to average over the lognormal shadowing. The simulations typically took several hours to generate a single point on the BER curve. Simulations are carried out with and without the cell-of-interest motion. When there is no cell motion, all the base stations are kept static, allowing only the mobiles to move. In the moving cell case, the base station B_{13} is allowed to move in a diagonal direction (as shown in Fig. 12) and also in a horizontal direction, keeping all the other base stations static. At each incremental movement of the cell-of-interest, a fresh reallocation of base stations to all the mobiles in the system is carried out. Note that the cell geometries become distorted and take random shapes when one accounts for base-station movement. The channel BER is estimated at different settings of the system simulation parameters, including number of users per cell, power-control update rate, vehicle speed, and the distance and direction of the cell-of-interest.

E. Static Base-Station Scenario Results

We first consider a single-cell system with flat Rayleigh fading ($L_p = 1$). Fig. 13 shows the simulated channel bit-error performance of the reverse link as a function of the number of active mobile users per cell, evaluated under conditions of no AWGN, $D = 0$, and $p_r = 0.0$. The performance curves are parameterized by different vehicle speeds (30 and 60 km/h) and update rates (800 Hz and 2 kHz). The performance curve for the system with no power control is also plotted for comparison. It is observed, as expected, that distinct

TABLE I
DS-CDMA SYSTEM CAPACITY WITH CLOSED-LOOP POWER CONTROL. FLAT RAYLEIGH FADING

Cell layout	Power control	Update rate	vehicle speed (km/h)	Capacity
Single cell	No	–	60	33
	Yes	800 Hz	60	60
			30	84
		2 KHz	60	97
			30	116
Multi-cell	No	–	60	23
	yes	800 Hz	60	39
			30	51
		2 KHz	60	60
			30	70

improvement in the channel BER is achieved when the vehicle speed is low (see curves for 30- versus 60-km/h speed) and the update rate is high (compare curves for 800- and 2-kHz update rates). From the above channel BER curves, the coded BER performance is obtained through (15) and (16). The necessary $\{\beta_i\}$ coefficients in (15) for the rate-1/3 convolutional code of constraint length 9 are taken from [24]. From the coded BER, the capacity of the reverse link is estimated (satisfying a coded BER of 10^{-3}, as typically required for voice) and is given in Table I. When there is no power control, the capacity achieved in a single-cell system is 33 simultaneous users. The capacity increases to 60 and 97 users when power control is applied at update rates of 800 Hz and 2 kHz, respectively, at 60-km/h vehicle speed.

Single-cell capacity estimates are optimistic, since they do not consider interference from other cell users. We estimated the capacity of a multicell DS-CDMA system with 25 cells configured in a square grid layout. The capacity of the multicell system is also shown in Table I. When there is no power control, the capacity achieved in a 25-cell system is 23 users, which corresponds to a 30% decrease in capacity compared to that of a single-cell system. With power control, at 60-km/h vehicle speed, the capacity increases to 39 users and 60 users for power-control update rates of 800 Hz and 2 kHz, respectively. Thus, there is a potential capacity improvement of the order of 50% when the update rate is increased from 800 Hz (used in IS-95) to 2 kHz. Note that these capacity estimates primarily indicate the effectiveness of the power control, without taking into account the effect of voice activity, antenna diversity at the base station, and sectorization.

The reverse link capacity of the CLPC scheme on a frequency-selective fading channel is now estimated. The number of independent, resolvable paths (L_p) is taken to be three. All the three paths are coherently combined using a three-tap (L_r) RAKE receiver. The exponent of the multipath intensity profile (μ) is taken to be 0.2. The total received powers for the cases of both flat and frequency-selective fading are kept constant. The estimated reverse link capacity for the above channel conditions, at different vehicle speeds and power-control update rates, are shown in Table II. Because

TABLE II
DS-CDMA SYSTEM CAPACITY WITH CLOSED-LOOP POWER CONTROL. FREQUENCY-SELECTIVE RAYLEIGH FADING. $L_p = L_r = 3$ AND $\mu = 0.2$

Cell layout	Power control	Update rate	vehicle speed (km/h)	Capacity
Single cell	No	–	60	75
	Yes	800 Hz	120	96
			60	103
			30	104
		2 KHz	240	105
			120	113
			60	114
Multi-cell	No	–	60	46
	yes	800 Hz	60	59

of the inherent diversity effect, capacities realized in the case of frequency-selective fading are found to be larger than in the flat fading case. For example, a single-cell system with no power control is found to support 75 simultaneous users on the reverse link when the channel is frequency selective as described above—this is a 2.2 times capacity improvement over the flat fading performance. When power control is applied, the capacity increases to 103 and 114 users for 800-Hz and 2-kHz update rates, respectively, at 60-km/h vehicle speed. This represents a capacity improvement of only 10% when the update rate is increased from 800 Hz to 2 kHz, which is in contrast to a 50% improvement in capacity when the channel fading is flat. This indicates that the capacity improvement due to faster update rates diminishes when the frequency selectivity of the channel increases. In a 25-cell square grid system, a capacity of 59 users is estimated for an 800-Hz update rate and 60-km/h vehicle speed. Note that we have assumed exact signal power measurement, perfect channel estimation, and maximal ratio combining at the RAKE receiver, and the capacities are expected to degrade from the currently estimated values in proportion to the imperfections involved in the measurements and combining.

F. Nonstationary Base-Station Scenario Results

In the nonstationary base-station scenario, we allow the cell-of-interest (cell with B_{13} as the base station) to move relative to adjacent cells, and estimate the reverse link capacity at the moving base station as a function of the degree of cell overlap and the direction of motion. Let q be the distance moved by the cell-of-interest. Because of the symmetry involved in the square grid layout, we evaluate the performance for the cases when the cell-of-interest moves in both horizontal and diagonal directions. Fig. 14 shows the coded BER performance under flat fading conditions at various degrees of cell overlap in the horizontal direction. The power-control update rate and vehicle speed considered are 800 Hz, and 60 km/h, respectively. The values of q considered are 0.0, 0.5, 0.707, and 0.9. Note that the value $q = 0.0$ corresponds to the static base-station scenario, and $q = 0.5$ corresponds to base station B_{13} being at the midpoint between its original static location and that of B_{14}. It is seen that when the cell-of-interest moves close to B_{14} (e.g., $q = 0.9$), the capacity degradation compared to the static base-station scenario ($q = 0.0$) is about 10% (39 users at $q = 0.0$ and 35 users when $q = 0.9$). The performance at the cell-of-interest when it is moved in a diagonal direction toward B_{19} between B_{14} and B_{18} is also evaluated. Here, the value $q = 0.707$ corresponds to the test base station being moved to the intersection of the cell boundaries of B_{14}, B_{18}, and B_{19}. A similar order of degradation is observed when the cell-of-interest is moved close to B_{19} (34 users when $q = 1.25$). Table III summarizes the variation of the system capacity as a function of the diagonal distance moved by the cell-of-interest, for both flat and frequency-selective fading.

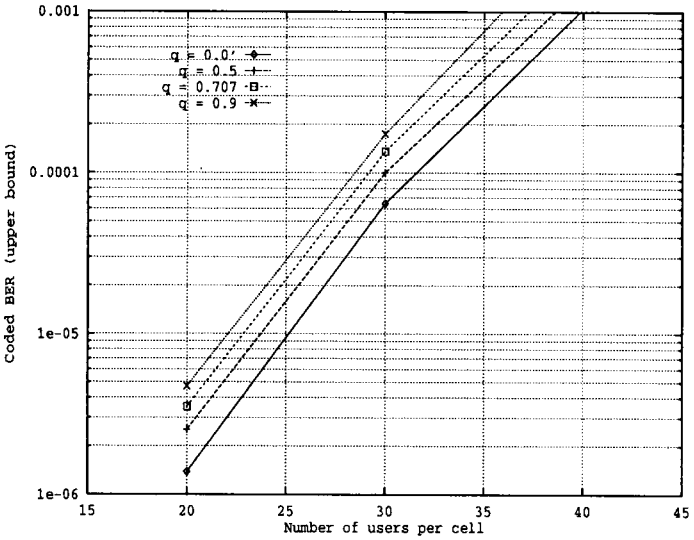

Fig. 14. Upper bound on the coded BER versus number of users per cell as a function of distance moved (in horizontal direction), $q = 0.0$, 0.5, 0.707, and 0.9. Flat Rayleigh fading. No AWGN. Power-control update rate = 800 Hz. $v = 60$ km/h.

TABLE III
SYSTEM CAPACITY AS A FUNCTION OF DISTANCE MOVED, q (IN DIAGONAL DIRECTION): FLAT FADING AND FREQUENCY-SELECTIVE FADING. $L_p = L_r = 3$ AND $\mu = 0.2$

Distance Moved (in diagonal direction)	System Capacity	
	Flat fading ($L_p = 1$)	Frequeny selective fading ($L_p = L_r = 3.\ \mu = 0.2$)
0.0	39	59
0.707	36	57
1.25	34	55

V. CONCLUSIONS

We derived a linear model for a CLPC system for DS-CDMA cellular communications. Analysis of the model indicated that it accurately predicts correlation times, but underestimates the magnitude of the correlation. This was primarily due to two of the modeling assumptions. To form a linear time-invariant system, we removed the sample-and-hold portion of the system model (mainly to allow a tractable analysis). Removing this portion in the model produces optimistic results because the mobile has better knowledge of the fading process than with the realistic model. Also, in deriving the noise input

to the linear system, we made an assumption that the received signal power term P_0 can be replaced by its desired value P_0^*, which was shown to yield optimistic results. The correlation times predicted in this analysis can be used in specifying coding and interleaving requirements. The present analysis can be extended to address the issue of bit-error correlation as well as burst error statistics approximations utilizing these correlation functions.

We also estimated the average BER on the reverse link as a function of various parameters in the power-control loop. The delay due to propagation and processing was shown to be the most critical parameter in the loop, and the error rate on the return channel to be the least critical. Using a quasi-analytic approach, we then estimated the capacity on the reverse link. The study emphasized the capacity improvement due to effective power control, and did not consider the effects of either voice activation or sectorization in the system model. It was shown that the performance on frequency-selective channels was significantly higher than that on flat fading channels. It was further shown that in a multicell environment under flat fading conditions, increasing the update rate from 800 Hz to 2 kHz resulted in a potential capacity improvement on the order of 50%. However, increasing the update rate resulted in diminishing capacity improvements as the channel became more and more frequency selective. The effect of nonstationary base stations on the reverse link capacity was also estimated. Typically, 10%–15% degradation in capacity was observed as the cell-of-interest moved close to adjacent base stations. Finally, the effect of imperfections in signal power measurement, channel estimation, RAKE combining, and synchronization on the current capacity estimates should be investigated as extensions to this work.

APPENDIX A
DERIVATION OF THE AUTOCORRELATION OF A_n

The flat fading amplitude from [17] follows a Rayleigh distribution. Following the traditional analysis, the fading process is generated from two independent Gaussian processes: X_n and Y_n. The power in the fading process Z_n is exponentially distributed (or chi-squared distributed with two degrees of freedom) with a pdf given by

$$f_{Z_n=X_n^2+Y_n^2}(z)=\frac{1}{2\sigma^2}\,e^{-(z/2\sigma^2)}.$$

The second-order statistics of the fading power loss in decibels

$$A_n=10\,\log_{10}\,Z_n$$

are required as inputs to the loglinear system model.

To find the correlation between A_i and A_j, a relationship between the Rayleigh product moments and the log-Rayleigh moment generating function is exploited

$$\begin{aligned}M_{A_i,A_j}(t_i,\,t_j)&=E[e^{t_iA_i}e^{t_jA_j}]\\&=E[Z_i^{(10/\ln 10)t_i}Z_j^{(10/\ln 10)t_j}].\end{aligned}$$

Simplifying a result from [18], the product moments of correlated Rayleigh random variables a_i, a_j generated from a Gaussian process, with inverse correlation matrix W, are

$$\begin{aligned}E[Z_i^\mu Z_j^\nu]&=E[a_i^{2\mu}a_j^{2\nu}]\\&=\frac{2^{(\mu+\nu)}||W||}{w_{11}^{(\mu+1)}w_{22}^{(\nu+1)}}\,\Gamma(1+\mu)\Gamma(1+\nu)\\&\quad\times{}_2F_1\left[(1+\mu),\,(1+\nu),\,1,\,\frac{w_{12}^2}{w_{11}w_{22}}\right]\end{aligned}\tag{A.1}$$

where ${}_2F_1$ is the hypergeometric function and w_{ij} is an element of the matrix W.

The underlying Gaussian random variables X_n and Y_n have identical variances, σ^2. The correlation coefficient between X_i and X_j (Y_i and Y_j), $\rho_{i,j}$, is a function of the Doppler spectrum of the radio channel. Replacing the elements of W by the corresponding expression in σ^2 and $\rho_{i,j}$, (A.1) reduces to

$$\begin{aligned}E[Z_i^\mu Z_j^\nu]&=2^{(\mu+\nu)}[(1-\rho_{i,j}^2)\sigma^2]^\mu[(1-\rho_{i,j}^2)\sigma^2]^\nu\\&\quad\times\Gamma(1+\mu)\Gamma(1+\nu){}_2F_1(1+\mu,\,1+\nu,\,1,\,\rho_{i,j}^2).\end{aligned}\tag{A.2}$$

The correlation, $E[A_i,\,A_j]$, is derived from the first partial derivative of (A.2), namely

$$\begin{aligned}E[A_iA_j]&=\frac{\partial^2}{\partial t_i\partial t_j}\,M_{A_i,\,A_j}(t_i,\,t_j)\bigg|_{t_i=0,\,t_j=0}\\&=\frac{100}{\ln^2\,10}\,\frac{\partial^2}{\partial\mu\partial\nu}\,E[Z_i^\mu Z_j^\nu]\bigg|_{\mu=0,\,\nu=0}.\end{aligned}$$

For simplicity, the above expression is broken into three pieces

$$E[A_iA_j]=\frac{100}{\ln^2\,10}\,\frac{\partial^2}{\partial\mu\partial\nu}\,f\cdot g\cdot h\tag{A.3}$$

where

$$\begin{aligned}f&\triangleq 2^{(\mu+\nu)}[(1-\rho_{i,j}^2)\sigma^2]^\mu[(1-\rho_{i,j}^2)\sigma^2]^\nu\\g&\triangleq\Gamma(1+\mu)\Gamma(1+\nu)\end{aligned}\tag{A.4}$$

and

$$h\triangleq{}_2F_1(1+\mu,\,1+\nu,\,1,\,\rho_{i,j}^2).$$

It can be verified that f and g have the following partial derivatives:

$$\begin{aligned}\frac{\partial}{\partial\mu}\,f&=2^{(\mu+\nu)}(1-\rho_{i,j}^2)[(1-\rho_{i,j}^2)\sigma^2]^{(\mu+\nu)}\\&\quad\times\,\ln[2(1-\rho_{i,j}^2)\sigma^2]\\\frac{\partial^2}{\partial\mu\nu}&=2^{(\mu+\nu)}(1-\rho_{i,j}^2)[(1-\rho_{i,j}^2)\sigma^2]^{(\mu+\nu)}\\&\quad\times\ln^2[2(1-\rho_{i,j}^2)\sigma^2]\\\frac{\partial}{\partial\mu}\,g&=\Gamma(1+\mu)\Gamma(1+\nu)\psi(1+\mu)\end{aligned}$$

and

$$\frac{\partial^2}{\partial\mu\nu}\,g=\Gamma(1+\mu)\Gamma(1+\nu)\psi(1+\mu)\psi(1+\nu)$$

where

$$\psi(x)=\frac{\partial}{\partial x}\,\ln\,[\Gamma(x)]$$

and, in particular

$$\psi(1) = -\boldsymbol{C}.$$

The constant $\boldsymbol{C}$ is the Euler Gamma constant and is approximately equal to 0.577 216. The partial derivatives of g are found by noting that for some function $f(u)$

$$\frac{\partial}{\partial u} f(u) = f(u) \frac{\partial}{\partial u} [\ln f(u)].$$

The partial derivatives of h are more difficult to compute. Utilizing the series expression for ${}_2F_1(1+\mu, 1+\nu, 1, \rho_{i,j}^2)$ [19, p. 1065], taking the partial derivative with respect to μ and setting $\mu = \nu = 0$ yields

$$\frac{\partial}{\partial \mu} {}_2F_1(1+\mu, 1+\nu, 1, \rho_{i,j})\bigg|_{\mu=\nu=0} = \sum_{k=0}^{\infty} \Gamma(1+k)[\psi(1+k) - \psi(1)] \frac{\rho_{i,j}^{2k}}{k!}. \quad \text{(A.5)}$$

Inserting the relationship [19, p. 954]

$$\psi(n+1) - \psi(1) = \sum_{j=1}^{n} \frac{1}{j} \quad \text{(A.6)}$$

into (A.5), exchanging the order of the summations, and simplifying yields

$$\frac{\partial}{\partial \mu} {}_2F_1(1+\mu, 1+\nu, 1, \rho_{i,j})\bigg|_{\mu=\nu=0} = -\frac{\ln(1-\rho_{i,j}^2)}{1-\rho_{i,j}^2}.$$

The partial derivative with respect to ν has the same value due to symmetry.

The partial derivative of h with respect to both ν and μ is

$$\sum_{k=0}^{\infty} \frac{\Gamma(1+\mu+k)}{\Gamma(1+\mu)} [\psi(1+k+\mu) - \psi(1+\mu)] \frac{\Gamma(1+\nu+k)}{\Gamma(1+\nu)} \times [\psi(1+k+\nu) - \psi(1+\nu)] \frac{\Gamma(1)}{\Gamma(1+k)} \frac{\rho_{i,j}^{2k}}{k!}.$$

Setting $\mu = \nu = 0$ and simplifying, it can be shown with significant effort that

$$\frac{\partial^2}{\partial \mu \nu} {}_2F_1(1+\mu, 1+\nu, 1, \rho_{i,j}) = \frac{\ln^2(1-\rho_{i,j}^2)}{1-\rho_{i,j}^2} + \frac{x\Phi(x, 2, 1)}{1-\rho_{i,j}^2}$$

where $\Phi(z, s, v)$ is defined in [19, p. 1103] as

$$z\Phi(z, 2, 1) = \sum_{n=1}^{\infty} \frac{z^n}{n^2} \quad \text{(A.7)}$$

and should not be confused with the Gaussian probability integral.

Using the product rule for differentiation, all of the partial derivatives computed in this section, and the values of f, g, and h, namely

$$f|_{\mu=\nu=0} = \sigma^2(1-\rho_{i,j}^2)$$
$$g|_{\mu=\nu=0} = -\boldsymbol{C}$$

and

$$h|_{\mu=\nu=0} = \frac{1}{1-\rho_{i,j}^2}$$

an expression for the correlation function results. After substantial algebraic simplification, we have

$$E[A_iA_j] = \frac{100}{\ln^2 10}[\rho_{i,j}^2 \Phi(\rho_{i,j}^2, 2, 1) + (\ln 2\sigma^2 - \boldsymbol{C})^2]. \quad \text{(A.8)}$$

Subtracting the product of the means of A_i and A_j yields the autocovariance function

$$\mathrm{Cov}[A_iA_j] = \frac{100}{\ln^2 10}[\rho_{i,j}^2 \Phi(\rho_{i,j}^2, 2, 1)] \quad \text{(A.9)}$$

where $\rho_{i,j}$ is the correlation coefficient of the underlying Gaussian processes X_i, X_j or Y_i, Y_j.

For the standard Doppler spectrum [17], the correlation coefficient for the process X or Y is

$$\rho_{i,j} \triangleq \frac{E[X_i, X_j]}{\sigma_x \sigma_y} = J_o[2\pi f_d (i-j) T_b]$$

where f_d is the Doppler bandwidth, and T_b is one bit duration. The resulting expression for $\mathrm{Cov}[A_i, A_j]$ becomes

$$\mathrm{Cov}[A_iA_j] = \gamma^2 J_o[\omega_d (i-j) T_b]^2 \big(\Phi\{J_o[\omega_d (i-j) T_b]^2, 2, 1\}\big) \quad \text{(A.10)}$$

where $\gamma = 10/\ln 10$ and $\omega_d = 2\pi f_d$.

Appendix B
Construction of the Noise Model—N_n

To characterize the noise input to the system N_n, an expression related to the power estimate error (in decibels) is derived. The signal power is estimated from the normalized square of the test statistic. Consider, without loss of generality, the test statistic for user zero. The test statistic for the ith bit is written as

$$g_0(iT_b) = \int_{iT_b - \tau_0}^{(i+1)T_b - \tau_0} 2S_r c_0(t-\tau_0) \cos(\omega_c t + \theta_0)\, dt$$

where

$$S_r = \sum_{l=0}^{K-1} \sqrt{2P_l} d_l(t-\tau_l) c_l(t-\tau_l) \cos(\omega_c t + \theta_l) + n(t).$$

The parameters P_l, c_l, d_l, τ_l, and θ_l are the lth user's received power, spreading sequence, data sequence, time delay, and carrier offset, respectively. The parameter K denotes the number of users. The thermal noise at the receiver is described by the AWGN process $n(t)$. Simplifying this expression in the standard fashion yields

$$g_0(iT_b) = T_b d_0^i \sqrt{2P_0} + I(iT_b) + N(iT_b) \quad \text{(B.1)}$$

where

$$I(iT_b) = \int_{iT_b - \tau_0}^{(i+1)T_b - \tau_0} \sum_{l=1}^{K-1} 2\sqrt{2P_l} d_l(t-\tau_l) c_l(t-\tau_l) \times c_0(t-\tau_0) \cos(\omega_c t + \theta_l) \cos(\omega_c t + \theta_0)\, dt$$

and

$$N(iT_b) = \int_{iT_b - \tau_0}^{(i+1)T_b - \tau_0} 2 \cos(\omega_c t + \theta_0) c_0(t-\tau_0) n(t)\, dt.$$

The received signal power estimate based on the normalized square of the test statistic is

$$\hat{P}_0 \triangleq \frac{g_0(iT_b)^2}{2T_b^2} = P_0 + \frac{[I(iT_b)+N(iT_b)]\sqrt{2P_0}}{T_b} + \frac{[I(iT_b)+N(iT_b)]^2}{2T_b^2}. \tag{B.2}$$

The analysis requires the error in the received power estimate in decibels. Thus, $10\log_{10} P_0$ is used to derive the loglinear estimate noise input process. However, the resulting expression is difficult to simplify due to a summation of terms within the logarithm.

Consider the following bounds derived from the convexity of the log function:

$$10\log_{10} P_0 + \frac{\gamma x}{x+P_0} \le 10\log_{10}(P_0+x) \le 10\log_{10} P_0 + \frac{\gamma x}{P_0}$$

where $\gamma = 10/\ln 10$. If P_0 is large compared to x, both expressions are close to the actual values, and either expression can be used as a good approximation. As x grows larger and approaches the magnitude of P_0, the bounds grow looser. Results indicate the bounds are tight if $x \le P_0/2$. The signal power P_0 is expected to be significantly larger than the interference terms x because of the use of power control, and therefore, both bounds form close approximations and only the upper bound is used as an approximation in what follows. A closer approximation can be obtained by considering a longer expansion for the log function. The issue of lower bounds and tighter approximations is not considered here.

Applying the above approximation to (B.2) and expanding the results gives

$$\hat{P}_{dB} = P_{dB} + \frac{\gamma}{T_b}\sqrt{\frac{2}{P_0}}\,[I(iT_b)+N(iT_b)] + \frac{\gamma}{P_0}\left[\frac{I(iT_b)N(iT_b)}{T_b^2} + \frac{I(iT_b)^2}{2T_b^2} + \frac{N(iT_b)^2}{2T_b^2}\right]. \tag{B.3}$$

From (B.3) surfaces an approximate definition for N_i in the loglinear system as

$$N_i \triangleq \frac{\gamma}{T_b}\sqrt{\frac{2}{P_0}}\,[I(iT_b)+N(iT_b)] + \frac{\gamma}{P_0}\left[\frac{I(iT_b)N(iT_b)}{T_b^2} + \frac{I(iT_b)^2}{2T_b^2} + \frac{N(iT_b)^2}{2T_b^2}\right]. \tag{B.4}$$

Conditioned on the value of P_0 and assuming the Gaussian approximation is valid for the interference term since the received powers of interfering users will be almost the same, N_i is a random variable having mean and variance given by

$$E[N_i|P_0] = \frac{\gamma}{2T_b^2 P_0}(\sigma_I^2+\sigma_N^2)$$

and

$$\mathrm{Var}[N_i|P_0] = \frac{\gamma^2}{P_0 T_b^2}\left(\frac{\sigma_I^2}{2} + \frac{\sigma_N^2}{2} + 2\sigma_I^2\sigma_N^2\right) + \frac{2\gamma^2}{T_b}(\sigma_I^2+\sigma_N^2)$$

respectively, with

$$\sigma_N^2 = N_0 T_b$$

and

$$\sigma_I^2 = \frac{2T_b^2}{3G}\sum_{l=1}^{K-1} P_l$$

where G is the processing gain and N_0 is the unilateral received noise power spectral density. Note that even conditioned on P_0, N_i is not a Gaussian random variable. The Gaussian assumption on $I(iT_b)$ is required to write the centralized fourth moment of $I(iT_b)$ as three times its variance. Inserting the expressions for the variances σ_I^2 and σ_N^2, and simplifying yields

$$E[N_i|P_0] = \gamma\left(\frac{N_0}{2E_b} + \frac{1}{3G}\sum_{l=1}^{K-1}\frac{P_l}{P_0}\right)$$

and

$$\mathrm{Var}[N_i|P_0] = 2\gamma^2\left(\frac{N_0}{2E_b} + \frac{1}{3G}\sum_{l=1}^{K-1}\frac{P_l}{P_0}\right)^2 + 4\gamma^2\left(\frac{N_0}{2E_b} + \frac{1}{3G}\sum_{l=1}^{K-1}\frac{P_l}{P_0}\right)$$

where E_b is the energy-per-bit.

To facilitate a tractable analysis, assume that the random term P_0 above is replaced by the desired value P^*. Using this approximation, the mean and variance reduce to

$$E[N_i|P_0] = \gamma\left(\frac{N_0}{2E_b^*} + \frac{1}{3G}\sum_{l=1}^{K-1}\frac{P_l}{P^*}\right) \tag{B.5}$$

and

$$\mathrm{Var}[N_i|P_0] = 2\gamma^2\left(\frac{N_0}{2E_b^*} + \frac{1}{3G}\sum_{l=1}^{K-1}\frac{P_l}{P^*}\right)^2 + 4\gamma^2\left(\frac{N_0}{2E_b^*} + \frac{1}{3G}\sum_{l=1}^{K-1}\frac{P_l}{P^*}\right). \tag{B.6}$$

In summary, the mean and variance of the process N_i were derived subject to two main approximations. The log approximation was examined explicitly, and seems to be a valid approximation when $P_0 > x$. If the log approximation is not accurate enough, additional terms in the log expan-

sion can be easily incorporated since the $N(iT_b)$ and $I(iT_b)$ terms are Gaussian. Approximating $I(iT_b)$ as Gaussian is a standard practice, but is a poor approximation for largely disparate power levels and small mobile populations. The second approximation, perhaps the most difficult to justify, is replacing P_0 by its desired value P^*. This removes some of the correlation present in the estimate error N_n. However, since the magnitude of P_0 will tend to vary, but remain close to P^*, this approximation is used to obtain a simple solution.

REFERENCES

[1] K. S. Gilhousen, I. M. Jacobs, R. Padovani, A. J. Viterbi, and L. A. Weaver, "On the capacity of a cellular CDMA system," *IEEE Trans. Veh. Technol.*, vol. 40, pp. 303–312, May 1991.

[2] R. W. Nettleton and H. Alavi, "Power control for a spread spectrum cellular mobile radio system," in *Conf. Rec. IEEE VTC'83*, 1983, pp. 242–246.

[3] S. Ariyavisitakul and L. F. Chang, "Signal and interference statistics of a CDMA system with feedback power control," *IEEE Trans. Commun.*, vol. 41, pp. 1626–1634, Nov. 1993.

[4] A. Chockalingam and L. B. Milstein, "Closed-loop power control performance in a cellular CDMA system," in *Conf. Rec., 29th Asilomar Conf. on Signals, Systems & Computers*, Nov. 1995, vol. 1, pp. 362–366.

[5] F. Simpson and J. Holtzman, "CDMA power control, interleaving, and coding," in *Conf. Rec. IEEE VTC'91*, St. Louis, MO, May 1991, pp. 362–367.

[6] J. Morris, "Burst error statistics of simulated Viterbi decoded BFSK and high-rate punctured codes on fading and scintillating channels," *IEEE Trans. Commun.*, vol. 43, pp. 695–700, Feb./Mar./Apr. 1995.

[7] H. Bischl and E. Lutz, "Packet error rate in the noninterleaved Rayleigh channel," *IEEE Trans. Commun.*, vol. 43, pp. 1375–1382, Feb./Mar./Apr. 1995.

[8] M. Werner, "Bit error correlation in Rayleigh fading channels," *Archiv fur Elektronik und Uebertragungstechnik*, vol. 44, no. 43, pp. 245–253, July 1991.

[9] S. Ariyavisitakul, "Signal and interference statistics of a CDMA system with feedback power control—Part II," *IEEE Trans. Commun.*, vol. 42, pp. 597–605, Feb./Mar./Apr. 1994.

[10] A. J. Viterbi, A. M. Viterbi, and E. Zehavi, "Performance of power-controlled wideband terrestrial digital communication," *IEEE Trans. Commun.*, vol. 41, Apr. 1993.

[11] P. Dietrich, R. R. Rao, A. Chockalingam, and L. B. Milstein, "Log-linear model for closed-loop power control," in *Conf. Rec. IEEE VTC'96*, Atlanta, Apr. 1996, vol. 1, pp. 51–55.

[12] G. L. Stuber and C. Kchao, "Analysis of a multiple-cell direct-sequence CDMA cellular mobile radio system," *IEEE J. Select. Areas Commun.*, vol. 10, pp. 669–679, May 1992.

[13] L. B. Milstein, T. S. Rappaport, and R. Barghouti, "Performance evaluation for cellular CDMA," *IEEE J. Select. Areas Commun.*, vol. 10, pp. 680–689, May 1992.

[14] A. Chockalingam and L. B. Milstein, "Performance of reverse link CDMA in a multicell environment with moving cells," in *Conf. Rec., IEEE MILCOM'95*, San Diego, Nov. 1995, vol. 3, pp. 937–941.

[15] W. C. Jakes, Ed., *Microwave Mobile Communication.* New York: Wiley, 1974.

[16] A. V. Oppenheim, A. S. Willsky, and I. T. Young, *Signals and Systems.* Englewood Cliffs, NJ: Prentice-Hall, 1983.

[17] R. H. Clarke, "A statistical theory of mobile radio reception," *Bell Syst. Tech. J.*, pp. 957–999, July–Aug. 1968.

[18] K. S. Miller, *Multidimensional Gaussian Distributions.* New York: Wiley, 1964.

[19] I. S. Gradshteyn, I. M. Ryzhik, and A. Jeffrey, Eds., *Table of Integrals, Series, and Products*, 5th ed. San Diego: Academic, 1994.

[20] R. Padovani, "Reverse link performance of IS-95 based cellular system," *IEEE Personal Commun.*, pp. 28–34, Third Quarter 1994.

[21] M. C. Jeruchim, P. Balaban, and K. S. Shanmugan, *Simulation of Communication Systems.* New York: Plenum, 1992.

[22] J. G. Proakis, *Digital Communications.* New York: McGraw-Hill, 1989.

[23] G. L. Turin *et al.*, "A statistical model of urban multipath propagation," *IEEE Trans. Veh. Technol.*, vol. VT-21, pp. 1–9, Feb. 1972.

[24] J. Conan, "The weight spectra of some short low-rate convolutional codes," *IEEE Trans. Commun.*, vol. COM-32, pp. 1050–1053, Sept. 1984.

A. Chockalingam (S'92–M'95) received the B.E. (Honors) degree in electronics and communication engineering from the P. S. G. College of Technology, Coimbatore, India, in 1984, the M.Tech. degree with specialization in satellite communications from the Indian Institute of Technology, Kharagpur, India, in 1985, and the Ph.D. degree from the Indian Institute of Science, Bangalore, India, in 1993. His Ph.D. thesis work was on design and performance evaluation of media-access protocols for wireless networks.

From 1986 to 1993, he was with the Transmission R&D Division of the Indian Telephone Industries Ltd., Bangalore, where he was involved in a range of R&D projects including VSAT networks using TDMA and CDMA, forward error correction, and variable-rate PSK modem implementations using ASIC and DSP technologies. From December 1993 to May 1996, he was a Post-Doctoral Fellow/Assistant Project Scientist at the Department of Electrical and Computer Engineering, University of California, San Diego, where he conducted research in CDMA wireless communications. He was a Communication Systems Consultant to CommQuest Technologies, Inc., Encinitas, CA, from 1994 to 1995. Since May 1996, he has been working with Qualcomm, Inc., San Diego, CA, where he is currently engaged in modeling and performance evaluation of CDMA wireless communication systems. His research interests are in the areas of wireless networks and digital communication systems.

Dr. Chockalingam is a Member of IETE.

Paul Dietrich received the B.S. degree in electrical engineering in 1990 from the Johns Hopkins University, Baltimore, MD, and the M.S. and Ph.D. degrees in electrical and computer engineering in 1991 and 1995, respectively, from the University of California, San Diego.

In January 1996, he received a Post-Doctoral position with the Center for Wireless Communications, University of California, San Diego. He is currently with Metricom. His research interests include network performance analysis, stochastic dependence, networks for parallel processing, packet communications over time-varying channels, and wireless MAC layer protocols.

Laurence B. Milstein (S'66–M'68–SM'75–F'85) received the B.E.E. degree from the City College of New York in 1964 and the M.S. and Ph.D. degrees in electrical engineering from the Polytechnic Institute of Brooklyn, Brooklyn, NY, in 1966 and 1968, respectively.

From 1968 to 1974, he was with the Space and Communications Group, Hughes Aircraft Company. From 1974 to 1976, he was a Member of the Department of Electrical and Systems Engineering, Rensselaer Polytechnic Institute, Troy, NY. Since 1976, he has been with the Department of Electrical and Computer Engineering, University of California, La Jolla, where he is a Professor and former Department Chairman, working in the area of digital communication theory with special emphasis on spread-spectrum communication systems. He has also been a Consultant to both government and industry in the areas of radar and communications.

Dr. Milstein was the Vice President for Technical Affairs in 1990 and 1991 of the IEEE Communications Society and has been a Member of the Board of Governors of both the IEEE Communications Society and the IEEE Information Theory Society. He was an Associate Editor for Communication Theory for the IEEE TRANSACTIONS ON COMMUNICATIONS, an Associate Editor for Book Reviews for the IEEE TRANSACTIONS ON INFORMATION THEORY, an Associate Technical Editor for the *IEEE COMMUNICATIONS MAGAZINE*, and is currently the Editor-in-Chief of the IEEE JOURNAL ON SELECTED AREAS IN COMMUNICATIONS. He is also a Member of Eta Kappa Nu and Tau Beta Pi.

Ramesh R. Rao (SM'90) was born in Sindri, India, in 1958. He received the Honors Bachelor's degree in electrical and electronics engineering from the University of Madras in 1980. He did his graduate work at the University of Maryland, College Park, receiving the M.S. degree in 1982 and the Ph.D. degree in 1984.

Since then he has been on the faculty of the Department of Electrical and Computer Engineering at the University of California, San Diego, where he is currently a Professor. He has been a Consultant to both industry and government in the area of networking. He is the Editor for Packet Multiple Access for the IEEE TRANSACTIONS ON COMMUNICATIONS. His research interests include architectures, protocols, and performance analysis of computers and communication networks.

Dr. Rao is a Member of the editorial boards of the *IEEE Network* and *ACM/Baltzer Wireless Networks Journal*. He is currently a Member of the Board of Governors of the IEEE Information Theory Society.